



# Hybrid optimized deep fuzzy clustering-based segmentation and Deep Maxout Network for Alzheimer's disease classification

T.S. Sindhu<sup>a,\*</sup>, N. Kumaratharan<sup>b</sup>, P. Anandan<sup>c</sup>

<sup>a</sup> Department of Electronics and Communication Engineering, C.Abdul Hakeem College of Engineering and Technology, Tamil Nadu 632509, India

<sup>b</sup> Department of Electronics and Communication Engineering, Sri Venkateswara College of Engineering, Tamil Nadu 602105, India

<sup>c</sup> Department of Electronics and Communication Engineering, Saveetha School of Engineering, Saveetha Institute of Medical and Technical Sciences, Saveetha University, Chennai, India

## ARTICLE INFO

### Keywords:

Deep Maxout network  
AD classification  
Deep fuzzy clustering  
Gaussian filter  
Data augmentation

## ABSTRACT

Alzheimer's disease (AD) is a type of dementia, which causes the neuron cell damages. The deep model is used to discover the quick and precise detection of AD. It has acquired immense interest for researchers, but the effective detection of AD with reliable biomarkers is a challenging task. A novel technique is developed using the deep model for AD classification. The Gaussian filter technique is used to remove the noise during the pre-processing stage. The next step is to segment the Region of Interest (RoI) using Deep Fuzzy Clustering (DFC) that has been optimized with the hyperparameters, which is tuned by the Sea Lion Deer Hunting Optimization (SLDHO) algorithm, which is developed by fusing the SLOA (Sea Lion Optimization Algorithm) and DHOA (Deer Hunting Optimization Algorithm). The features such as textual features, CNN (Convolutional Neural network) features and statistical features are obtained. For better processing, more suited data are used and the augmentation of data is performed. The classification process is done based on the Deep Maxout network (DMN), and it is trained by the developed SLDHO model. Additionally, the DMN classifies AD into five types Cognitive Impairment (MCI), Early Mild Cognitive Impairment (EMCI), AD, Mild Cognitively Normal (CN), and Late Early Mild Cognitive Impairment (LMCI). The DFC-SLDHO-based DMN outperformed with the maximum specificity, sensitivity and accuracy of 89.8 %, 84.4 % and 87.4 %.

## 1. Introduction

A form of dementia known as AD is also known as a neurodegenerative illness since it specifically harms neuron cells. The total number of patients increases progressively and also causes death in some cases. There exist several hypotheses regarding AD's pathway, and several drugs are devised for slowing or stopping the rate of disease [10,1]. AD is a disease, which poses a dangerous onset. It is featured by inclusive dementia in such a way that aphasia, a disorder in memory, agnosia and apraxia are caused [11]. With the population ages, AD tends to be a burden globally in the upcoming days [4]. AD is an irreversible, degenerative and incurable dementia that causes patients to mislay existing capabilities. It is estimated that 85 individuals are affected by AD [12]. The patients suffering from AD have an enormous burden on the economy and also hit patients and their families. According to literary techniques, MCI subjects transition to AD at a rate of 10–15 % [13,3] whereas Normal Controls (NC) focus on AD patients. The quick

and precise discovery of AD based on structural Magnetic Resonance Imaging (MRI) has produced imperative notice among researchers that owes to deep learning techniques [2].

Because of its astounding oath, enhanced contrast and increased accessibility, Magnetic Resonance Imaging (MRI) has recently become widely employed in hospitals for diagnosing AD [14]. Although early AD diagnosis has improved, predicting development and exploration using structural MRI is still challenging [2]. Positron Emission Tomography (PET), structural magnetic resonance imaging (MRI) and functional magnetic resonance imaging (fMRI) are just a few of the techniques that have been heavily modified in recent years for AD/MCI studies [15]. In addition, machine learning techniques have devised emerging performances in several applications that involve biomedical tools. The structural MRI offer information regarding the kind of tissue of the brain and turn out to be a strong tool for the assessment of AD patients because of apparent differences and elevated spatial decision [16,33,35]. The structural magnetic resonance imaging is generally used for the

\* Corresponding author.

E-mail addresses: [sindhuts1992@gmail.com](mailto:sindhuts1992@gmail.com) (T.S. Sindhu), [kumaratharan@rediffmail.com](mailto:kumaratharan@rediffmail.com) (N. Kumaratharan).

<https://doi.org/10.1016/j.bspc.2024.106118>

Received 16 November 2023; Received in revised form 30 January 2024; Accepted 14 February 2024

Available online 1 March 2024

1746-8094/© 2024 Elsevier Ltd. All rights reserved.

assessment of steady neural provocation. It incarcerates fundamental variation in the brain and captures unavoidable damages caused, because of neurodegeneration of AD alkalosis [17,7]. The majority of techniques determined the process of degradation and it affected the areas of the brain, like the hippocampus by using sMRI. The modality of MRI is positioned on the progress of water molecules and termed as Diffusion Tensor Imaging modality (DTI) [7]. The sMRI can perceptively capture the anatomical brain changes, which are considered an effectual tool for disease diagnosis [8].

There exist no drugs which treat AD earlier and on the other hand accurate treatment of AD is more essential. Recently, deep and machine learning models have been used to resolve complicated issues. Classical Machine Learning techniques are devised based on statistics and mine features from raw data [136]. In [18,4], structured sparse kernel learning technique, Single-Nucleotide Polymorphism (SNP) features and Positron Emission Tomography (PET). There are deep learning-based techniques for detecting AD [19,4]. A deep learning model ensemble using landmarks is devised for diagnosing [20,8]. An ensemble technique is used that combines various classifiers based on various local patches [21]. The efficiency of classification can be suboptimal as several patches are inputted to each classifier that ignores the interface of various patch features [8]. In [22,7], a classification model for the longitudinal assessment of MRI images for the treatment of AD is developed based on merging Recurrent Neural Network (RNN), CNN [34], and Multi-Layer Perceptron (MLP). Pre-processing, image segmentation, feature extraction, feature selection, and classification are the important steps in the multi-staged model [23,7]. The technique processes the MRI into various segments during the pre-processing stage. For constructing the similarity matrices vector, the technique used Grey Matter (GM) as the Region of Interest and exactly GM statistical features were mined.

### 1.1. Motivation

AD is a kind of brain disorder. It slowly damages the brain's memory and thinking skills. Also, it causes brain cell damage. There are many methods have been invented for AD classification. The major challenges of the existing methods are given below:

- Most of the AD classification techniques required more iteration for the training process which consumed more time.
- In the existing methods, most of the optimal parameters in AD classification are data-dependent to obtain the open problem automatically.
- In some existing methods, the data segmentation is not optimal. It decreases the volume of the estimation's accuracy and the significance of the result.

These are the common issues in the previous traditional approaches, which are considered as the motivation for developing the DFC + SLDHOA-based DMN technique.

The main aim of this research is to develop a clustering technique for AD classification that is driven by optimization. Then, the pre-processing is done by the input data after they are obtained from a dataset. Gaussian filter is adapted to remove redundant pixels and artifacts from input images in pre-processing. After ROI segmentation is processed by using DFC, the hyperparameters are tuned by the SLDHO model, and it is the integration of DHOA and SLOA. Then, features extraction is used to extract the statistical features like mean, entropy, variance, skewness, contrast, energy, kurtosis, and standard deviation. Also, textual features like Local Gabor Binary Pattern (LGBP) and Spider Local Image Features (SLIFs), respectively. At last, the classification process is done based on DMN, which is trained by SLDHO. Here, the developed SLDHO-based DMN classifies AD into five types such as EMCI, LMCI, MCI, CN and AD.

The novelty of this research is as follows:

- **Proposed SLDHO-based DFC for ROI segmentation:** The SLDHO-DFC model is developed for the segmentation process. The pre-processing is done by using the Gaussian filter. Then, the pre-processed image is fed into ROI segmentation, and it is obtained by the proposed SLDHOA on DFC. Moreover, the SLDHO is obtained by combining the DHOA and SLOA for tuning the hyperparameters of DFC to generate effective segments.
- **Proposed SLDHO-based DMN for AD classification:** In this research, the proposed SLDHO-based DMN is developed to classify the AD. Further, the DMN model is trained by the developed SLDHO algorithm. Moreover, the DMN classifies AD into five types, namely MCI, LMCI, AD, CN and EMCI.

The organization of the paper is given as follows: Section 2 illustrates the motivation, literature review and challenges. The developed AD classification technique is presented in Section 3. Section 4 describes the results and comparative discussion. Finally, the conclusion is illustrated in Section 5.

## 2. Motivation

The person who suffers from Alzheimer's is susceptible to accidental falls and are at high risk for life-threatening injuries. Thus, designing an efficient AD model for the above-mentioned challenges and issues is referred to as motivation.

### 2.1. Literature review

This section illustrates the issues and advantages based on various techniques of AD. Minseok Song *et al.* [1] devised an RF technique with a huge count of sub-trees for classifying AD using MRI data. The RF with three feature sets was modified in this instance to categorize AD. The RF technique detected the AD more reliably with fewer features. This method attains a specificity of 83.5 %, a sensitivity of 73.3 %, and an accuracy of 81.6 %, respectively. Nevertheless, this method was unable to predict the stages of disease progression. Jong Bin Bae *et al.* [2] classified the MRI data from two groups that varied in terms of education level and ethnicity and were used to create a Convolutional Neural Network (CNN). Here, the T1-weighted images were covered by the medial temporal lobe. Also, this method was achieved by the fast support tools for AD. The obtained value of this method was 84.4 % of accuracy, 78.9 % of sensitivity, and 89.1 % of specificity. The main issue of this method was high processing time. LinaXu *et al.* [3] developed a manifold regularized sparse regression model to learn the discriminative features. Here,  $\ell_{2,1}$  norm regularization was adapted for jointly choosing the pertinent feature among the samples. Here, the regularization term was devised using relative distance for adjusting label information that can handle intra- and inter-class samples. Further, this method was done with the binary and the multi-class classification. Also, this method achieved better classification performance. The values of accuracy, sensitivity and specificity were 84.3 %, 77.5 %, and 88 %, respectively. However, this technique did not utilize parameter optimization for fixing the optimum parameter.

Yuanpeng Zhang *et al.* [4] developed an AD multiclass classification model using fusion based on multimodal neuroimaging and embedding selection of features. For selecting the best features, they used  $\ell_{2,1}$  multiclass hinge loss with norm regularization. The complementary data were then merged with different kernels for multiple kernel processing. By integrating  $\ell_{2,1}$  norm and  $\ell_p$ -norm regularizations, it was possible to minimize multiclass hinge loss. However, this technique was not available to optimize the norms. Xin Bi *et al.* [5] devised a technique for classifying the AD. Two deep learning algorithms were developed based on functional brain networks. The extreme learning machine was used to improve learning ability. Moreover, the deep regional connectivity features were used to learn the convolutional learning method, while the deep adjacent positional features were used to learn the recurrent

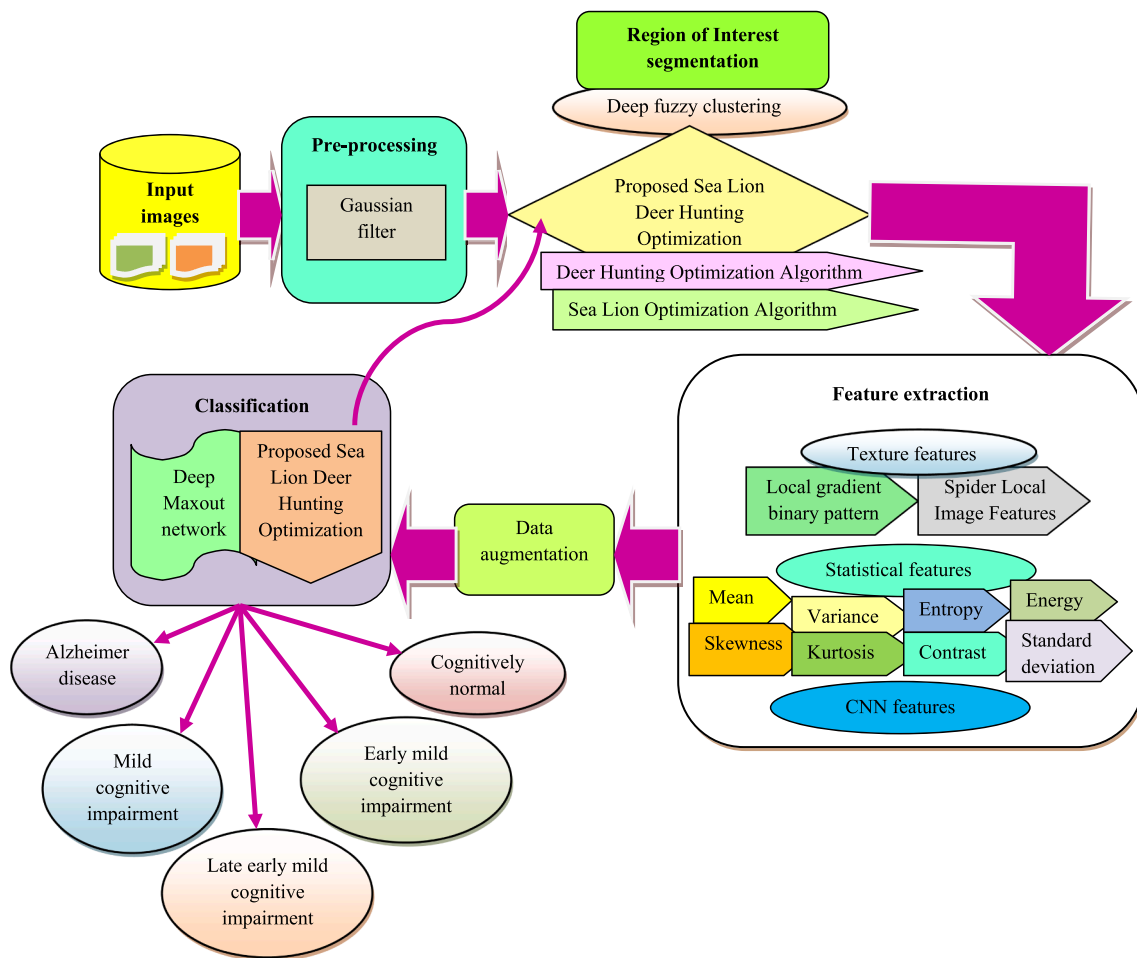


Fig. 1. Structure of proposed SLDHOA-based DMNin AD classification.

learning method. However, different RoI positions can affect efficiency. To identify AD, Himanshu Padole et al. [6] developed a two-stage graph coarsening technique based on graph signal processing. Here, Graph Wavelet Transforms (GWT)-based features were utilized for obtaining a graph. In this method, the coarsening problem was evaluated by using the optimization problem to reduce the Laplacian operator level and increase the topological similarity. This method obtained a specificity of 89.4 %, sensitivity of 80.9 %, and an accuracy of 85.4 %. However, this technique computed less accuracy. By using a pre-trained AlexNet model, Sitara Afzal et al. [7] introduced a Transfer Learning (TL)-based efficient technique for accurately categorizing the multi-class AD. Here, two methods for seeing the brain and viewing the brain in three dimensions were created. This model attained a value of specificity of 89.6 %, a sensitivity of 82.8 %, and an accuracy of 86.1 % respectively. However, this technique required more iteration for training which consumed more time. Tian Zhu et al. [8] developed a Directed Acyclic Graph (DAG)-based classification technique for diagnosing AD. Here, the anatomical feature patches were detected by statistical and morphological assessment. A powerful DAG CNN was developed for mining discriminative deep features for representing images. Then, by combining map features with different network levels, the deep features were created. After that, the AD was classified using a support vector machine. This method, however, failed to take actual environmental factors.

## 2.2. Challenges

In an existing AD classification technique, the issues are illustrated as

follows,

- Optimum administration of agitation in AD forms a major issue for avoiding delay and enhances the quality of life of patients [9].
- The Manifold regularized sparse regression model is devised in [3] for AD detection, but this technique did not adopt other structural features, like area and volume that comprise commentary data.
- Multi-modal neuro-imaging embedding feature selection and fusion approach is devised in [4] for classifying the AD. However, this technique poses a certain issue that involves huge subjects, and the accumulation of kernel matrix needs huge space.
- In [8], the DAG network and anatomical landmarks are devised for detecting AD, but this technique failed to design binary classification for automated diagnosis of various brain diseases.
- The Extreme Learning Machine and Deep Features are utilized for detecting AD. However, these types of techniques failed to explore graph theory-based features for improved learning.

In this research, the DFC + SLDHOA-based DMN model is implemented to address the challenges of these existing methods. Here, the Gaussian filter removes the image artifacts, which increases the accuracy. Also, DFC is more comprehensive and is used to analyze large-scale datasets. Moreover, the integration of SLnO and DHOA improves the overall algorithmic performance. The mining of characteristics ensures accurate AD classification. The overfitting issues are avoided by the data augmentation procedure. Besides, the DMN converges quickly and generalizes the results in an optimal manner.

**Table 1**  
SLDHOA-based DFC pseudo code.

SLDHOA-based DFC pseudo code
Input: $K = \{h_1, h_2, \dots, K_i, \dots, K_h\}$
Output: Feature vector $C$
Initialize the fuzzy clustering center $\lambda$ , bias $S$ , and weight $E$
while ( $epoch\ number \leq Iter_{max}$ ) do
for ( $batch\ number \in [1, m/m_c]$ ) do
Detect $P_g$ , reconstruction $ER_{YZ}(A_g)$
Find the objective function using equation (3)
Evaluate the fuzzy memberships $M_{ij}$
Find the target $K_v$
Derive the KL loss of function
Find the graph regularization using equation (7)
Derive the final loss of function using equation (8)
end for
for ( $batch\ number \in [1, a/a_c]$ ) do
Update $L_v$
end for
end while
End

### 3. SLDHO-based DMN for AD classification

AD is a dementia, and it is also called a neurodegenerative condition. The patients tend to maximize the steadily and thereby the disease is considered as a global issue, which can even cause death. This research aims to devise a technique for classifying AD. The Gaussian filter is used to pre-process the input image. After that, ROI segmentation is done using DFC [25] in which the parameters are tuned by the proposed SLDHOA. Accordingly, the proposed SLDHOA is devised by integrating DHOA [26] and SLOA [27]. In image segmentation, the segmented image is mined for CNN features, and textual features like LGBP [28] and SLIF [29]. Moreover, the statistical features are kurtosis, energy, mean, entropy, contrast and variance skewness. Performance is enhanced through data augmentation using extracted features. At last, the AD classification is done using DMN [24], which is trained using the SLDHO algorithm. Additionally, the types of AD are classified using the DMN model into five categories such as MCI, LMCI, EMCI, CN, and AD. The structure of Alzheimer's disease classification using SLDHOA-based DMN is shown in Fig. 1.

Consider the dataset of an image  $F, h$  denotes the images and it is mathematically represented as,

$$F = \{K_1, K_2, \dots, K_i, \dots, K_h\} \quad (1)$$

where  $K_i$  is represented as the  $i^{th}$  image of input,  $h$  symbolizing the number of images.

#### 3.1. Gaussian filter for noise removal using preprocessor

Here, the pre-processing phase receives the  $i^{th}$  input image and  $K_i$  as an input. In the process of evaluating the input images, the pre-processing is regarded as a crucial step. Pre-processing is a crucial step in image processing, which makes it appropriate for categorizing AD. Additionally, the pre-processing removes any image artifacts that may be present. The pre-processing stage is fed into the image enhancement process because it can enhance the difference of the image for AD classification. Here, image noise is reduced by modifying the Gaussian filter.

##### (i) Gaussian filter

The noise in an image is removed using the Gaussian filter [31]. The filter can provide smoother progress in the frequency domain. Also, this filter performs well since it may deliver noise reduction and smooth transition. Also, the Gaussian filter, which processes the images by using the Gaussian functions, is represented as,

$$G(P, Q) = \frac{1}{\sqrt{2\pi\eta^2}} e^{-\frac{P^2+Q^2}{2\eta^2}} \quad (2)$$

Where the standard deviation is represented as  $\eta$ , also  $P, Q$  symbolize the filter kernel size  $J(-J \leq P, Q \leq J)$ . ROI segmentation from the pre-processed image  $K'_i$ .

#### 3.2. ROI segmentation using SLDHOA-based deep fuzzy clustering

The  $K'_i$  is used as an input in segmentation of ROI. By using SLDHOA-based DFC, which is generated by fusing the SLDHOA and DFC, the  $K'_i$  is sent to segmentation. Thus, the segments are obtained based on interesting regions in which each segment represents individual regions. By helping to define borders and objects, the ROI segmentation increases their significance and value. Here, the ROI segmentation is done using SLDHOA-based DFC. In this method, the hyperparameters are determined using SLDHOA, which is obtained by combining DHOA and SLnO. The DFC and steps of SLDHOA are included.

##### 3.2.1. Deep fuzzy clustering

The pre-processed output  $K'_i$  is supplied into the DFC [25] as input. Here, the DFC is obtained by integrating the DFC with the SLDHOA such that allows the SLDHOA to determine the hyperparameter of the DFC. Assume, that the DFC is  $F' = \{K'_1, K'_2, \dots, K'_i, \dots, K'_h\}$ , an input pre-processed image has been acquired with the cluster numbers  $d$ , size of batch  $m_c$  and the maximum of iteration  $Iter_{max}$  as indicated. The partitioning samples  $F$  into  $m/m_c$  batches and a training image  $K_i, i = 1, 2, \dots, m/m_c$  is given for each image. Additionally, when training the autoencoder considers weights is denoted as  $\omega$  and bias is denoted as  $D$  into account and is chosen  $\lambda$  as the fuzzy clustering center. The  $Q_v$  is represented as hidden features, fuzzy in memberships are represented as  $I_v$  and pseudo labels are calculated  $I_v$  for initialize the affinities in all batches  $L_v \in \mathbb{R}^{m_c \times m_c}$ . The loss of function is given by,

$$O(K\theta) = \frac{1}{m} \sum_{i=1}^m \|x_{E,S}(K_i) - K_i\|^2 + \eta \cdot Y(E) \quad (3)$$

Where the Euclidean norm is written as  $Y(E)$  denotes the regularization and the reconstruction term is written as  $x_{E,S}(h_i)$ . Assume the hidden representation  $g_i \in \mathbb{R}^q$  and  $Q = \{g_1, g_2, \dots, g_i, \dots, g_m\}$ . In the fuzzy clustering layer, the input  $g_i$  and the fuzzy membership  $M_{ij}$  are given as,

$$M_{ij} = \frac{\left( \|g_i - \lambda_j\|^2 - \frac{\gamma}{\sum_{\tau=1}^q \|\lambda_\tau - \bar{\lambda}\|^2} \|\lambda_j - \bar{\lambda}\|^2 \right)^{-1/(a-1)}}{\sum_{\tau=1}^q \left( \|g_i - \lambda_\tau\|^2 - \frac{\gamma}{\sum_{\tau=1}^q \|\lambda_\tau - \bar{\lambda}\|^2} \|\lambda_\tau - \bar{\lambda}\|^2 \right)^{-1/(a-1)}} \quad (4)$$

where,  $\gamma$  is denoted as a hyperparameter of cluster distance and cluster space, and express fuzzification is denoted as  $a$ . The labels of pseudo  $k_v$  are mined  $I_v$  and  $K_v$  denoted as the target and it is evaluated as,

$$K_{ij} = \frac{M_{ij}^2 / \sum_i M_{ij}}{\sum_{\tau=1}^q (M_{i\tau}^2 / \sum_i M_{i\tau})}, \sum_{j=1}^q K_{ij} = 1 \forall i \quad (5)$$

The loss of function for KL-divergence is,

$$\min KL(K||I) = \min \sum_{i=1}^m \sum_{j=1}^q K_{ij} \log \frac{K_{ij}}{M_{ij}} \quad (6)$$

The representation of the regularization of graph is,

$$\min H_g = \min \sum_{i,l=1}^m \|g_i - g_l\|^2 p_{il} \quad (7)$$

Here,  $p_{il}$  expresses affinity among  $K_i$  and  $K_l$ . When affinity among  $K_i$  and  $K_l$  is high the distance between  $h_i$  and the small regularization is represented as  $g_l$ . At last, the loss of function  $B_v$  is expressed as,

$$B = \sum_{i=1}^m \|x_{E,S}(h_i) - h_i\|_2^2 + \beta_1 \sum_{i=1}^m \sum_{j=1}^q K_{ij} \log \frac{K_{ij}}{M_{ij}} + \beta_2 \sum_{i,l=1}^m \|g_i - g_l\|^2 p_{il} \quad (8)$$

$$p_{il} = \begin{cases} \exp(-\|g_i - g_l\|^2 / \kappa) / \chi; & \ell_i = \ell_l \\ 0 & ; \ell_i \neq \ell_l \end{cases} \quad (9)$$

where, the hyperparameters are  $\beta_1$  and  $\beta_2$ ,  $\kappa$  signifies the kernel which is fixed to 1,  $\chi$  refers hyperparameter of affinity and  $\ell_i$  expresses the label of pseudo code and  $\ell_l$  signifies the label. Table 1 describes SLDHOA-based DFC pseudo code.

$\beta_1, \beta_2, \gamma, \chi$  and the fuzzifier  $m$  are the parameters, discovered with SLDHOA in SLDHOA-based DFC. The steps of SLDHOA are given below.

### 3.2.2. SLDHOA-based training for tuning hyperparameters in DFC

The proposed SLDHOA, which is devised by fusing DHOA and SLnO is used to tune the hyperparameters in DFC. DFC is used to evaluate several circumstances; also, it is more comprehensive and is used to analyze large-scale datasets. The DHOA [26] is inspired by deer qualities and wants to protect them from hunters. The DHOA hunting methodology is then created based on the movement of optimal to hunter place. The benefits of DHOA are, used to solve the test problem and it is more competitive compared to other types of algorithms. The exploitation and exploration phases are balanced by the DHOA model. Also, the DHOA has the searching ability for attaining the favorable regions is observed to be high. Also, the behavior of convergence in DHOA is good compared to other metaheuristic algorithms. The SLnO [27] is inspired by the sea lions' natural liability for hunting. Additionally, the SLnO takes its devise cues from the whiskers used by sea lions to find their prey. It is aggressive and has few parameters, which helps with both exploration and exploitation. In contrast to iterations, the SLnO has a high convergence speed and evaluates the avoidance of raised local best solutions. The advantages of SLnO are, when working on different benchmark functions, the SLnO algorithm provides very competitive results compared with other optimization algorithms. SLnO evaluates the best solution and also contains the high speed of convergence. Thus, the integration of DHOA and SLnO improves the overall algorithmic performance. To enhance the overall algorithmic performance, SLnO and DHOA are thus integrated. The SLDHOA steps are given below.

Step 1) Population Initialization:

SLDHOA uses the initial solution as a first, and it is expressed by,

$$M = \{M_1, M_2, \dots, M_j, \dots, M_g\}; 1 \leq j \leq g \quad (10)$$

Where the hunters are represented as  $g$ .

Step 2) Detection of the loss function

In equation (3), the loss function is already described.

Step 3) Initialization of algorithmic parameter

As per DHOA [26], the angle of wind and the angle of deer position are imperative for describing the best position of hunters. It is given as,

$$\phi_f = 2\pi q \quad (11)$$

Where, a random number in [0, 1] is denoted as  $qf$  is represented as the iteration. The Deer's angle is expressed by,

$$\zeta = \phi + \pi \quad (12)$$

Where wind angle is represented as  $\phi$ .

Step 4) Position Propagation

The method ensures that the candidate solution is nearer to the optimal solution In this case, the two solutions such as successor and leader position are used.

#### a) Propagation via leadership position

The optimum position of each endeavor is expressed as,

$$M_{f+1} = M^{lead} - N \cdot t \cdot |T \times M^{lead} - M_f| \quad (13)$$

where,  $M_f$  represents the position of the deer in iteration, and  $M_{f+1}$  represents the position of the deer in the next iteration, a random number between [0, 2] signifies  $t$ ,  $N$  and  $T$  signify coefficient vectors.

The vector of coefficient is given as,

$$N = \frac{1}{4} \log \left( f + \frac{1}{f_{max}} \right) r \quad (14)$$

where,  $f_{max}$  implies iteration in maximum, the parameter between  $-1$  and  $1$  is  $r$ .

The vector of coefficient is given as,

$$T = 2 \cdot s \quad (15)$$

Where random integer between [0,1] is referred to as  $s$ .

The mathematical expression is,

$$M_{f+1} = M^{lead} - N \cdot t \cdot (T \times M^{lead} - M_f) \quad (16)$$

$$M_{f+1} = M^{lead} - N \cdot t \cdot T \times M^{lead} - N \cdot t \cdot M_f \quad (17)$$

$$M_{f+1} = M^{lead} (1 - N \cdot t \cdot T) - N \cdot t \cdot M_f \quad (18)$$

According to SLnO [27], sea lions hunt bait balls of fish beginning at the boundaries and expressed as,

$$M_{f+1} = |K_f - M_f| \cdot \text{Cos}(2\pi m) + K_f \quad (19)$$

where the target vector represents  $K_f$ , the vector of sea lion is written as  $M_f$ , a random number in  $[-1, 1]$  is referred as  $m$  and  $\text{Cos}(2\pi m)$  describes a sea lion swimming in circles shaped the path for hunting prey is written as.

Assume  $K_f > M_f$ ,

$$M_{f+1} = (K_f - M_f) \cdot \text{Cos}(2\pi m) + K_f \quad (20)$$

$$M_{f+1} = K_f \cdot \text{Cos}(2\pi m) - M_f \cdot \text{Cos}(2\pi m) + K_f \quad (21)$$

$$M_{f+1} = K_f (\text{Cos}(2\pi m) + 1) - M_f \cdot \text{Cos}(2\pi m) \quad (22)$$

**Table 2**

Pseudo code of SLDHOA.

Pseudo code of SLDHOA
<b>Input:</b> Population $M$
<b>Output:</b> Optimum solution $M_{f+1}$
<b>Begin</b>
<b>While</b> ( $f < f_{\max}$ )
<b>for</b>
Calculate the fitness function
Update the algorithmic parameters
<b>if</b> ( $Z < 1$ )
<b>if</b> ( $ X  \geq 1$ )
Update the leader position by using equation (30)
<b>else</b>
Update the successor position based on equation (35)
<b>end if</b>
<b>Else</b>
Update the solution with position angle by equation (34)
<b>end if</b>
<b>end for</b>
Derive fitness function
Update $M^{\text{lead}}$ and $M^{\text{successor}}$
$f = f + 1$
<b>End while</b>
<b>Return</b> $M^{\text{lead}}$
Terminate

$$K_f = \frac{M_{f+1} + M_f \cdot \cos(2\pi m)}{\cos(2\pi m) + 1} \quad (23)$$

As  $K_f$  is the target prey position in SLNo, it can be substituted in the leader position of DHOA  $M^{\text{lead}}$ . Thus, substitute equation (23) in equation (18) is given as,

$$M_{f+1} = \frac{M_{f+1} + M_f \cdot \cos(2\pi m)}{\cos(2\pi m) + 1} (1 - N \cdot t \cdot T) - N \cdot t \cdot M_f \quad (24)$$

$$M_{f+1} = \frac{M_{f+1}}{\cos(2\pi m) + 1} (1 - N \cdot t \cdot T) + \frac{M_f \cdot \cos(2\pi m)}{\cos(2\pi m) + 1} (1 - N \cdot t \cdot T) - N \cdot t \cdot M_f \quad (25)$$

$$M_{f+1} - \frac{M_{f+1}}{\cos(2\pi m) + 1} (1 - N \cdot t \cdot T) = \frac{M_f \cdot \cos(2\pi m)}{\cos(2\pi m) + 1} (1 - N \cdot t \cdot T) - N \cdot t \cdot M_f \quad (26)$$

$$M_{f+1} \left( 1 - \frac{(1 - N \cdot t \cdot T)}{\cos(2\pi m) + 1} \right) = \frac{M_f \cdot \cos(2\pi m)}{\cos(2\pi m) + 1} (1 - N \cdot t \cdot T) - N \cdot t \cdot M_f \quad (27)$$

$$M_{f+1} \left( \frac{\cos(2\pi m) + 1 - 1 + N \cdot t \cdot T}{\cos(2\pi m) + 1} \right) = \frac{M_f \cdot \cos(2\pi m)}{\cos(2\pi m) + 1} (1 - N \cdot t \cdot T) - N \cdot t \cdot M_f \quad (28)$$

$$M_{f+1} \left( \frac{\cos(2\pi m) + N \cdot t \cdot T}{\cos(2\pi m) + 1} \right) = \frac{M_f \cdot \cos(2\pi m)}{\cos(2\pi m) + 1} (1 - N \cdot t \cdot T) - N \cdot t \cdot M_f \quad (29)$$

The updated equation of the proposed SLDHOA is given as,

$$M_{f+1} = \frac{(\cos(2\pi m) + 1)M_f}{\cos(2\pi m) + N \cdot t \cdot T} \left[ \left( \frac{\cos(2\pi m)}{\cos(2\pi m) + 1} (1 - N \cdot t \cdot T) - N \cdot t \right) \right] \quad (30)$$

### b) Propagation via position angle

The following is the visualization angle for deer or prey.

$$\ell_f = \frac{\pi}{8} \times b \quad (31)$$

A parameter is calculated by comparing the angle of the deer and its visual angle, which is written as,

$$C_f = \phi_f - \ell_f \quad (32)$$

Where wind angle is referred to as  $\phi$ .

The position of angle update is given as,

$$\zeta_{f+1} = \zeta_f + C_f \quad (33)$$

By using position angle, the updated position is given as,

$$M_{f+1} = M^{\text{lead}} - t \cdot |\cos(e) \times M^{\text{lead}} - M_f| \quad (34)$$

### c) Propagation via successor position

The updated position of successor is written as,

$$M_{f+1} = M^{\text{successor}} - N \cdot t \cdot |T \times M^{\text{successor}} - M_f| \quad (35)$$

Where the position of successor is signified as  $M^{\text{successor}}$ .

### Step 5) Acquisition of the best solution

When a new solution that is associated with the least value is used to adjust the hyperparameters, the loss value of that solution is computed.

### Step 6) Terminate:

The above-mentioned processes are repeatedly carried out until the optimum answer is found. The Pseudo code of the developed SLDHOA is explained in Table 2.

The SLDHOA-based DMN offered segments are denoted as  $R$ .

### 3.3. Acquisition of significant features

The extracted feature from each segment after collecting the segments  $R$ . The mining of characteristics ensures accurate classification of AD. The characteristics covered here include CNN features and statistical features. The statistical features include kurtosis, skewness, variance, standard deviation, mean, contrast, entropy and energy. Also, the texture features such as LGBP and SILF features, respectively.

#### (i) Texture features

The images are segmented into interesting regions and in these regions, then, the texture features are extracted.

#### (a) LGBP

The basic idea of LGBP [28] is that instead of adjusting LBP on raw images, LBP is applied to Gabor input images. To create the LGBP feature, all of the energy image histogram characteristics are adjusted. The LGBP operator has a higher feature size than the LBP operator. The plots of image pixels in LBP operator with  $\lambda_p (p = 0, 1, \dots, 7)$  nearest pixel thresholding  $3 \times 3$  using the mid-value  $\lambda_c$ . Furthermore, the LGBP operator refers to the integration of extraction and Gabor filtering of LBP features. The threshold value in binary form is represented using an image as follows:

$$\mathfrak{N}(\lambda_p - \lambda_c) = \begin{cases} 1, & \lambda_p \geq \lambda_c \\ 0, & \lambda_p < \lambda_c \end{cases} \quad (36)$$

The pattern of LBP in pixel is then given as follows,

$$LBP = \sum_{p=0}^7 \mathfrak{N}(\lambda_p - \lambda_c) 2^p \quad (37)$$

This  $C_1$  is expressed as the LGBP feature.

#### (b) SLIF

The multi-kernel SLIF [29] is employed to address the issues that occur at the time of the image-matching process. The selectively mining details of images are used to detect the feature from the predicted feature point. Thus, multi-kernel SLIF is mined from the pre-processed image for effectual AD. The multi-kernel SLIF model processes are given by,

- The SLIF orb web sampling design

The orb web modeling is used to adapt all discovered points to mine the information of pixels from the key points of neighborhood, after that the equal feature descriptor is created by utilizing the mined pixel details. The expression of orb web structure is,

$$A^j = \left\{ \vec{v}_{o,z}^j \mid o = 1, 2, \dots, O ; z = 1, 2, \dots, Z \right\} \quad (38)$$

Where the position of the web node is expressed as  $I_{o,x}^j$ . Additionally, the orb web structure location must be changed to fit a feature point. Each node's position  $(o, z)^j$  in the shifted orb web structure  $A^j$  is determined by,

$$\vec{v}_{o,z}^j = \left( a_j + \frac{z \cdot \cos\left(\frac{2\pi o}{O}\right)}{Z}, y_j + \frac{z \cdot \cos\left(\frac{2\pi o}{O}\right)}{Z} \right) \quad (39)$$

Where, the coordinates of vertical and horizontal image are represented as  $a_j$  and  $y_j$ 'th point of interest. The position of nodes should be enhanced to adjust various alternations and expressed as,

$$\vec{v}_{o,z}^j = \left( a_j + \frac{T \cdot \mu_j \cdot z \cdot \cos\left(\frac{2\pi o}{O}\right)}{Z}, y_j + \frac{T \cdot \mu_j \cdot z \cdot \cos\left(\frac{2\pi o}{O}\right)}{Z} \right) \quad (40)$$

Where the feature scale in key-point implies  $\mu_j$ , and the positive scalar factor is represented as  $T$ .

Finally, the SLIF feature should have the ability to control the rotations of the image to exact the rotation-invariant feature descriptions, which is done by including all orientation information for the essential points in the representation of orb web, which is represented as,

$$\vec{v}_{o,z}^j = \left( a_j + \frac{T \cdot \mu_j \cdot z \cdot \cos\left(\frac{2\pi o}{O} + \varphi_j\right)}{Z}, y_j + \frac{T \cdot \mu_j \cdot z \cdot \cos\left(\frac{2\pi o}{O} + \varphi_j\right)}{Z} \right) \quad (41)$$

where,  $\varphi_j$  express orientation of key-point.

- Information sampling and web weight assignment

The information extraction in the feature point is processed again and utilized to create a collection of equivalent feature vectors. The benefits of competent distribution of web nodes are adapted for mining imperative data of pixel intensity from neighborhoods of particular interest points. Additionally, the data of pixel intensity is reduced at each node location  $N_{c,d}^e$  in the orb web structure by using a unique Gaussian kernel to prevent aliasing.

$$H_{o,z}^j = A \left( N_{o,z}^j \right) \times T_z^j(\phi) \quad (42)$$

Where,

$$T_z^j(\phi) = B_z^j(\phi) + M_z^j(\phi) \quad (43)$$

where,  $A \left( N_{o,z}^j \right)$  refers to the data of pixel intensity from an image  $A$  at a specific web node location  $N_{o,z}^j$ ,  $B_z^j(\phi)$  expresses Gaussian kernel, and  $M_z^j(\phi)$  signifies the kernel size and linear kernel is given as,

$$S_k = \frac{P \cdot \phi_j \cdot z}{2 \cdot O} \quad (44)$$

Where, the scale of feature is referred to  $P$ , and  $\phi$  is expressed as the standard deviation. The value of the standard deviation is 0.5.

- Orientation assignment

It is used to identify the interest point in a depicted image, which is evaluated for orientation angle. Also, every web node's equivalent 2D-directed vector of influence is given by,

$$\vec{J}_{o,z}^{j} = \left[ Y_{o,z}^j \cdot \cos\left(\frac{2\pi o}{O}\right), Y_{o,z}^j \cdot \sin\left(\frac{2\pi o}{O}\right) \right] \quad (45)$$

where a web node's connection to the web weight denotes  $Y_{o,z}^j$ . Each vector's vectorial total is then calculated and stated as,

$$\vec{J}^j = \sum_{o=1}^O \sum_{z=1}^Z \vec{J}_{o,z}^{j} \quad (46)$$

#### iv) SLIF's descriptor construction

The obtained feature  $\varpi$  is then analyzed using the specific point as follows,

$$\varpi_j = [s_{1,1}^j, s_{2,1}^j, \dots, s_{O,1}^j, s_{1,1}^j, s_{2,1}^j, \dots, s_{O,2}^j, \dots, s_{1,Z}^j, s_{2,Z}^j, \dots, s_{O,Z}^j] \quad (47)$$

Where the 8 bit binary array denotes the values of  $s_{o,x}^j$ . In addition, every byte  $s_{o,x}^j$  is coded by including a collection of 8 bit binary standards. It is expressed as,

$$s_{o,z}^j = \{s_{o-1,z+1}^j, s_{o,z+1}^j, s_{o+1,z+1}^j, s_{o-1,z}^j, s_{o+1,z}^j, s_{o-1,z-1}^j, s_{o,z-1}^j, s_{o+1,z-1}^j\} \quad (48)$$

Where the numbers  $s_{o+p,z+q}^j$  stand for binary bits that  $p, q \in (-1, 0, 1)$  are allotted to compare the certain pair of web weight values.  $H_{o,z}$  and  $H_{o+p,z+q}$  are written as,

$$s_{o+p,z+q}^j = \begin{cases} 1 & \text{if } H_{o,z}^j > H_{o+p,z+q}^j \\ 0 & \text{otherwise} \end{cases} \quad (49)$$

The point allocation is altered to achieve the desired feature descriptor dimension, allowing for more detailed and specific feature descriptors to be created.  $C_2$  is denoted as the output of multi-kernel SLIF.

#### (ii) 4 Statistical features

Variance, Mean energy, entropy, standard deviation, skewness, contrast and kurtosis are some of the statistical features that have been

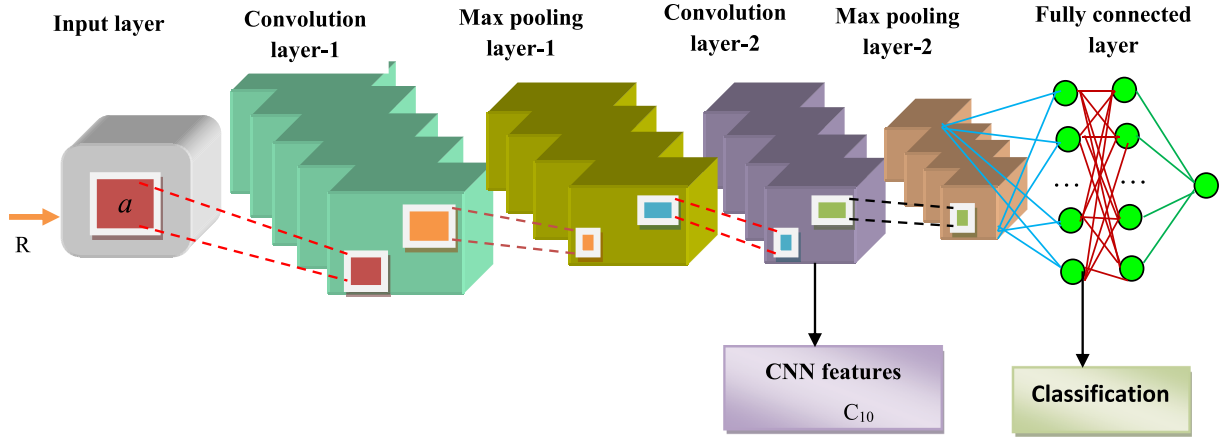


Fig. 2. The Structure of CNN with feature extraction and classification.

utilized for characterizing image content. The following are illustrations of each feature:

(a) Mean

The term “Mean” which is obtained by calculating the average of pixels in the image is mathematically represented as,

$$\mu = \frac{1}{|d(Y_n)|} \times \sum_{n=1}^{|d(Y_n)|} d(Y_n) \quad (50)$$

Where the total segments signify  $n, d(Y_n)$  is denoted as the values of pixel in each segment and total pixels contained in the segment are referred to as  $|d(Y_n)|$ .  $C_3$  is expressed as a mean feature.

(b) Variance

The term “Variance” is detected by the mean value and is given by,

$$\sigma = \frac{\sum_{n=1}^{|d(Y_n)|} |Y_n - \mu|}{d(Y_n)} \quad (51)$$

The feature of variance is denoted as  $C_4$ .

(c) Standard deviation

Standard deviation  $C_5$  represents the variance in square root.

(d) Entropy

The Image’s entropy is calculated by pixel and is given by,

$$E(\rho_L, \rho_Z) = \sum_{Y=1}^{u(\rho_L)} P(\rho_L = L, \rho_Z = Z) \cdot \log(\rho_L = L, \rho_Z = Z) \quad (52)$$

where  $E(\rho_L, \rho_Z)$  represents the image pixel entropy,  $u(\rho_L)$  refers to the values of unique pixels and  $(L, Z)$  refers pixel location of the image.  $C_6$  denotes the feature of entropy.

(e) Energy

By combining the energies of the pixels within a segment, the energy feature of each segment is mined. The segment’s energy comes from,

$$\varepsilon = \sum_{o=1}^{|\rho(L_o)|} \varepsilon(Y_o) \quad (53)$$

This  $C_7$  is denoted as an energy feature.

(f) Skewness

The smoother and darker surfaces are more skewed than lighter and duller surfaces. As a result, skewness is used to make decisions about image surfaces. The skewness is represented by  $C_8$ .

(g) Kurtosis

Kurtosis expresses evenness that describes peak sharpness. The Kurtosis feature is denoted as  $C_9$ .

(h) Contrast

By analyzing various variations in brightness or color that make a different object, the different feature is produced. The contrast is stated as follows:

$$C = \frac{\ell}{\kappa} \quad (54)$$

Where,  $\ell$  signifies the difference of luminance and  $\kappa$  expresses average luminance. The feature of contrast is denoted as  $C_{10}$ .

(iii) CNN features

CNN feature denotes a neural network model, which contains various layers, such as three leaky relu layers, four max-pooling layers, four convolution layers, and three dense layers. The fine-tuning of CNN [32] understands features more effectively. CNN’s main characteristics include weight sharing, spatial sharing and local connection.

The segments of the convolution layer  $J$  as input and CNN features as output, which is expressed  $C$  with a dimension of  $[1 \times 2048]$ . The output of the function in convolution is given by,

$$C(k) = (a * W(k)) \quad (55)$$

Where  $a$  implies the input of CNN,  $C(k)$  is represented as a map feature and  $W(k)$  represents function in probability density or kernel. The CNN feature is denoted as  $C_{11}$ . Fig. 2 reveals the Structure of CNN with feature extraction and classification.

#### 4.0.1. Configuration of feature vector

The vector feature is given by,

$$C = \{C_1, C_2, C_3, C_4, C_5, C_6, C_7, C_8, C_9, C_{10}, C_{11}\} \quad (56)$$

Where  $C_1$  symbolizes the LGBP feature,  $C_2$  represents the SLIF feature,  $C_3$  signifies the mean feature,  $C_4$  refers variance feature,  $C_5$  is the Standard deviation feature,  $C_6$  is the Entropy feature,  $C_7$  is the

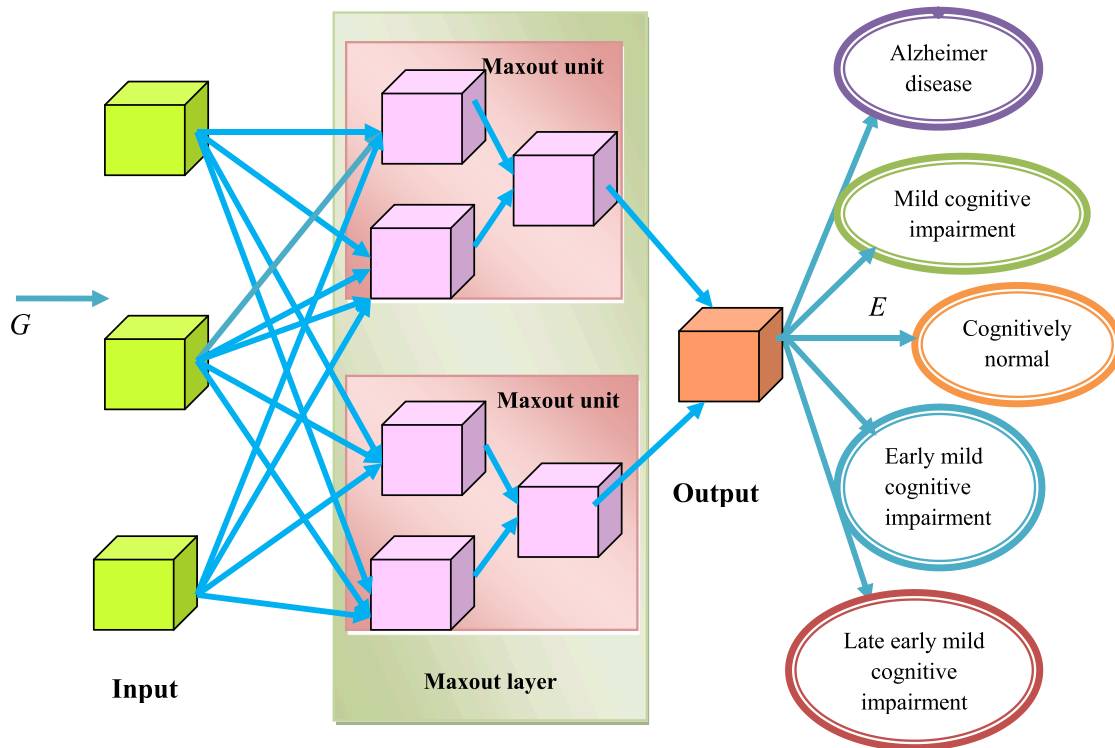


Fig. 3. Structure of DMN with Multi-layer structured Maxout.

Energy feature,  $C_8$  is the Skewness feature,  $C_9$  is Kurtosis feature  $C_{10}$  is contrast feature, and  $C_{11}$  express CNN (Convolutional Neural Network) features.

#### 4.1. Data augmentation

The vector feature  $C$  is fed to data augmentation [33]. Here, data augmentation is carried out utilizing three techniques, such as feature standardization, zero-phase component analysis (ZCA) whitening and random rotations, shifts and flips.

##### (i) Feature standardization

The feature standardization is done to uniform the pixel value throughout the whole database. It reflects the type of standardization that is frequently applied to each column of a tabular database. The Image Data Generator class is used to conduct feature standardization by specifying the feature-wise center and feature-wise STD normalization arguments.

##### (ii) ZCA whitening

The pixel image matrix's redundancy is reduced via the whitening transformation of the image, which is a linear algebraic operation. Lesser redundancies of the image help to better spotlight the features and image structures. Moreover, the whitening image is done using the Principal Component Analysis (PCA) method.

##### (iii) Random rotations, shifts and flips

The random rotations, shifts and flipping of each image data are described below.

##### (a) Rotations

The images in the data can be altered and contain different rotations

among the scene. The model can be trained to manage the image rotations by randomly and artificially rotating images. Here, the image can be rotated left and right up to 90 degrees.

##### (b) Shifts

Sometimes, the objects in images are not centered and can be off-center in various ways. Thus, the off-center objects can be handled by artificially creating shifted versions. Here, the vertical and horizontal random shifting is done using `height_shift_range` and `width_shift_range` arguments, which thereby builds shifted versions of the digits.

##### (c) Flips

The flipping helps to enhance the performance on huge and complicated issues by creating random flips of images. Here, the random flipping is done on both horizontal and vertical axes considering `vertical_flip` and `horizontal_flip` arguments. This helps in adjusting the varied orientation. Thus,  $G$  is represented as the output of data augmentation.

#### 4.2. SLDHOA-based DMN for AD classification

The AD classification is performed with DMN and the detection is carried out with the augmented data  $G$ , which is obtained from the previous step. Here, DMN is trained with the help of the SLDHOA algorithm which is newly proposed in this paper.

##### 4.2.1. Structure of DM

The DMN [24] comprises Maxout units that assist in simplifying functions and assists to produce optimal solutions with elevated accuracy. Furthermore, in comparison to other networks, the DMN model converges quickly and generalizes the optimal manner that is straightforward to optimize. The Maxout networks perform better at averaging models. The DMN takes the advantage of numerous non-saturated activation functions and trainable functions. By switching to inactive, Maxout enables an optimization mechanism by avoiding hidden units.

Finally, the input sent to DMN is represented as  $G$ . Fig. 3 represents the DMN structure with a multi-layer structured Maxout.

A multilayer model that includes trainable activation functions is called a DMN. Given input  $x \in R^d$  where  $x$  denotes a hidden layer's state vector or a raw input vector, the activation of a hidden unit is specified as,

$$g_{ij}^1 = \max_{j \in [1, k_1]} x^T \omega_{ij} + h_{ij} \quad (57)$$

$$g_{ij}^2 = \max_{j \in [1, k_2]} g_{ij}^{1T} \omega_{ij} + h_{ij} \quad (58)$$

$$g_{ij}^m = \max_{j \in [1, k_m]} g_{ij}^{m-1T} \omega_{ij} + h_{ij} \quad (59)$$

$$g_{ij}^n = \max_{j \in [1, k_n]} g_{ij}^{n-1T} \omega_{ij} + h_{ij} \quad (60)$$

$$g_i = \max_{j \in [1, k_n]} g_{ij}^n \quad (61)$$

Here  $k_m$  represents the units in the  $m^{\text{th}}$  layer,  $n$  represents the number of layers in the DMN, and  $\omega_{ij}$  represents the weights and  $h$  represents the bias. The DMN training is carried out with SLDHOA, which is described below.

#### 4.2.2. 3.5.2. DMN Training

The steps present in SLDHOA are described.

##### Step 1) Population Initiation:

The initialization is the first step of the solution in the SLDHOA, and it is denoted as,

$$M = \{M_1, M_2, \dots, M_j, \dots, M_g\}; 1 \leq j \leq g \quad (62)$$

Where,  $g$  implies the number of hunters.

##### Step 2) Error Determination

Mean Square Error (MSE) is used to choose the optimal solution, which is calculated using the output error and applied to the problem of minimization. So, MSE is described as,

$$MS_{err} = \frac{1}{g} \sum_{h=1}^g [\xi_h - E]^2 \quad (63)$$

where  $g$  denotes the number of data samples,  $\xi_h$  symbolizes predicted output and  $E$  expresses output acquired through DMN, like  $1 < h \leq g$ .

##### Step 3) Update equation detection

The SLDHOA's derivation is already detailed in section 3.2.2. The SLDHOA's final update equation is given as,

$$M_{f+1} = \frac{(\cos(2\pi m) + 1)M_f}{\cos(2\pi m) + N \cdot t \cdot T} \left[ \left( \frac{\cos(2\pi m)}{\cos(2\pi m) + 1} (1 - N \cdot t \cdot T) - N \cdot t \right) \right] \quad (64)$$

##### Step 4) Calculating errors to update solutions:

The new solution error is evaluated, and associated weights with the lowest error are used to train the DMN.

##### Step 5) Finish:

The maximum iteration is obtained by generating the optimal weights regularly. Thus, the output of SLDHOA-based DMN is represented as  $E$ , where denotes one of five possible types: MCI, LMCI, EMCI, CN and AD.

**Table 3**  
Parameter Details.

Parameters	Values
Batch_size	32
Embedding_dimension	50
Filters	50
Kernel_size	3
Epochs	20
Padding	'valid'
Activation	'relu'
Strides	1
Loss	'categorical_crossentropy'
Optimizer	SLDHOA
Metrics	Accuracy, sensitivity, specificity

## 5. Results and discussion

By varying the training data, the proposed DFC + SLDHOA-based DMN is assessed in terms of specificity, sensitivity, and accuracy.

### 5.1. Experimental setup

The DFC + SLDHOA-DMN is implemented in Python and runs on Windows 10 with an Intel core processor and 2 GB RAM. The parameter details of the proposed model are explained in Table 3.

### 5.2. Dataset description

The Alzheimer's-Disease-5-Class-Dataset-ADNI is used for the analysis [30]. These data contain two directories of MRI images which are then divided into the five stages of AD for testing and training of AD, MCI, LMCI, and EMCI which are the five stages of AD CN and AD.

### 5.3. Experimental outcomes

Fig. 4 presents the experimental results of the proposed DFC + SLDHOA-DMN for AD classification. Fig. 4a) displays the input image acquired from the dataset. Fig. 4b) reveals the pre-processing image. Fig. 4c) depicts the segmented images obtained using modified DFC, and Fig. 4d) presents the LGBP image.

### 5.4. Evaluation measures

A few metrics, which are discussed below, are used to adjust the outcome of the AD classification.

#### 5.4.1. Accuracy

In the classification of AD, the term "accuracy" relates to how closely the calculated value resembles the actual value and is given as,

$$Accuracy = \frac{Y^p + Z^n}{Y^p + Y^n + Z^p + Z^n} \quad (65)$$

where  $Y^p$  symbolizes the true positive,  $Y^n$  signifies the true negative,  $Z^p$  denotes the false positive and  $Z^n$  refers to the false negative.

#### 5.4.2. Sensitivity

The term "sensitivity" expresses the positive ratio which is noticed by the AD classification method as,

$$Sensitivity = \frac{Y^p}{Y^p + Z^n} \quad (66)$$

#### 5.4.3. Specificity

The term "specificity" refers to the ratio of precisely recognized negatives using the suggested model.

$$Specificity = \frac{Y^n}{Y^n + Z^p} \quad (67)$$

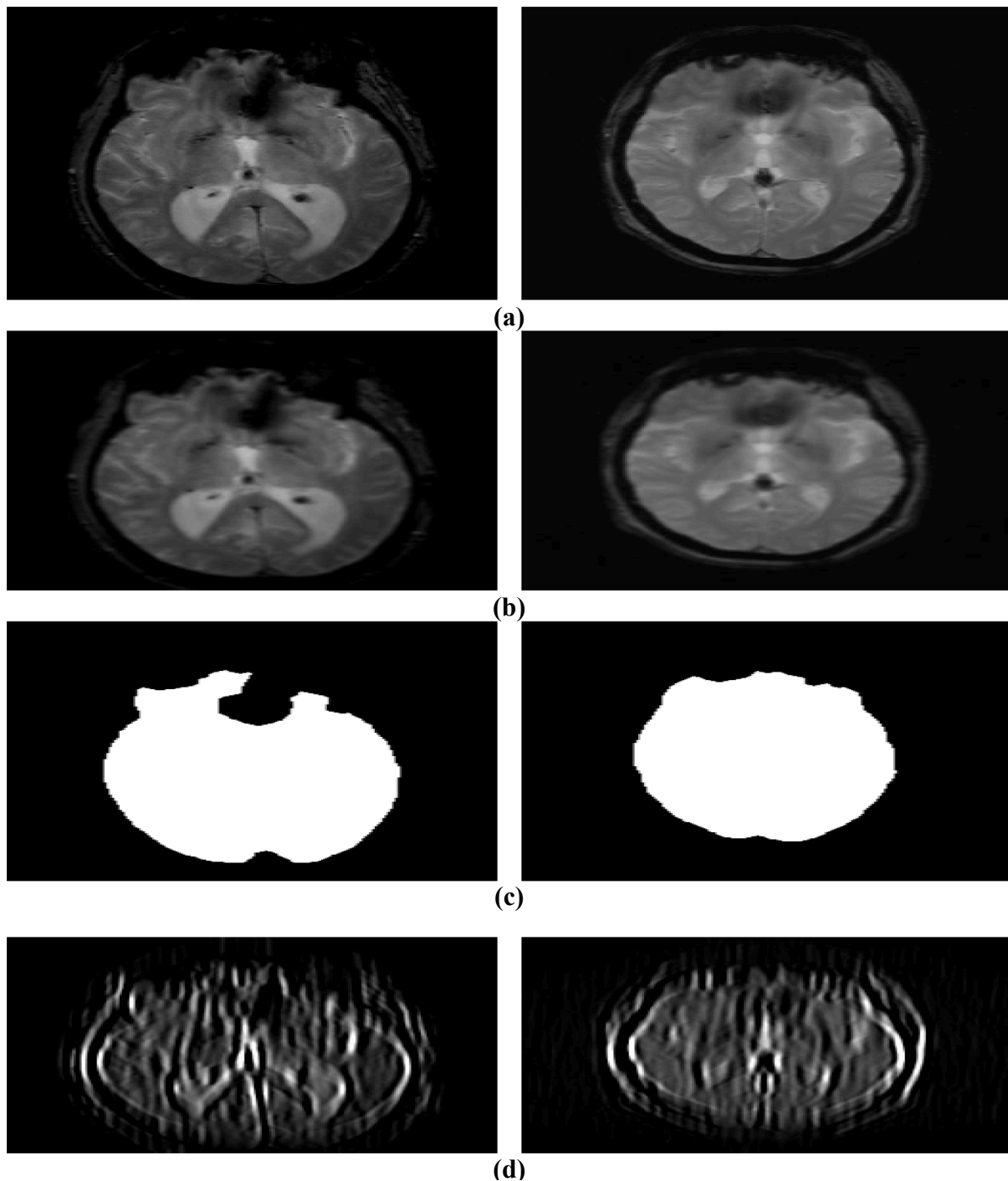


**Fig. 4.** Experimental results of the developed DFC + SLDHOA-based DMN a) Input image, b) Pre-processed image, c) Segmented image, and d) LGBP image.

### 5.5. Performance analysis

By adjusting training data utilizing population sizes of 10 and 15, the evaluation of DFC + SLDHOA-based DMN's accuracy, sensitivity and specificity are described.

#### 5.5.1. Estimation with population size of 10

Fig. 5 represents the Evaluation of the DFC + SLDHOA-based DMN with a population size of 10. Fig. 5 a) explains the accuracy of DFC + SLDHOA-DMN with a population size of 10. DFC + SLDHOA-based DMN with hidden neurons = 100, 200,300 and 400 computed accuracy 50 %

of data is 45.3 %, 45.8 %, 49.5 % and 49.6 % respectively. Additionally, for 90 % of data, DFC + SLDHOA-based DMN with hidden neurons = 100, 200, 300, and 400. For each of the four data sets, the accuracy was 83.7 %, 84 %, 85.6 % and 87.3 %. Fig. 5b) shows the mean segmentation accuracy of DFC + SLDHOA-based DMN with a population size of 10. For AD class type, the mean segmentation accuracy evaluated by DFC with cluster size = 2, 3, 4, 5 are 81.2 %, 81 %, 80.5 % and 80.4 %. Also, for the MCI class type, the mean segmentation accuracy evaluated by DFC with cluster size = 2, 3, 4, 5 are 86.6 %, 86 %, 85.9 % and 83.2 %. Fig. 5c) shows the sensitivity of DFC + SLDHOA-based DMN with a population size of 10. According to DFC + SLDHOA-based DMN with hidden neurons = 100, 200, 300 and 400, the sensitivity of 50 % of data

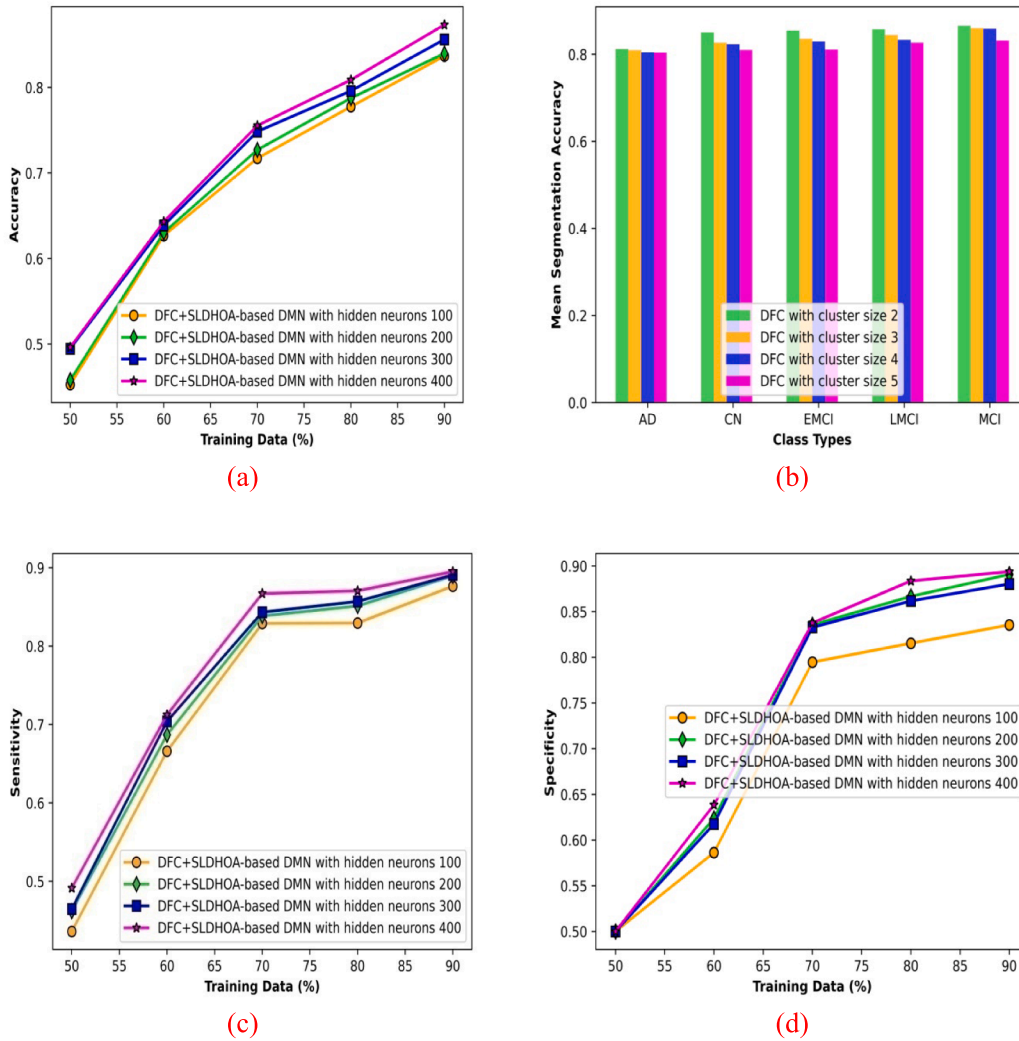


Fig. 5. Performance evaluation of the DFC + SLDHOA-DMN with population size = 10 using a) Accuracy b) Mean segmentation accuracy c) Sensitivity d) Specificity.

is 43.6 %, 46.2 %, 46.5 % and 49.1 %. In addition, for 90 % of data, DFC + SLDHOA-based DMN with hidden neurons = 100, 200, 300 and 400 rated sensitivity as 87.6 %, 88.9 %, 89.1 % and 89.5 %, respectively. Fig. 5 d) depicts the specificity of DFC + SLDHOA-based DMN with a population size of 10. The specificity determined by DFC + SLDHOA-based DMN with hidden neurons = 100, 200, 300 and 400 is 50 %, 50 %, 50 % and 50 % for 50 % of data. Additionally, for 90 % of data, DMN based on DFC + SLDHOA with hidden neurons = 100, 200, 300 and 400 evaluated the specificity at 83.5 %, 89.1 %, 88 % and 89.4 %.

### 5.5.2. Estimation with population size of 15

Fig. 6 illustrates the assessment of DMN based on DFC + SLDHOA with a population size of 15. Fig. 6 a) represents the accuracy of DFC + SLDHOA-based DMN with a population size equal to 15. The accurateness measured by the DFC + SLDHOA-based DMN with hidden neurons = 100, 200, 300 and 400 is 46.3 %, 47.1 %, 48 % and 49.1 % for 50 % of data. Additionally, the DFC + SLDHOA-based DMN with hidden neurons = 100, 200, 300 and 400 has accuracy evaluations of 81.9 %, 82.4 %, 83.9 % and 86.4 % for 90% of the training data. Fig. 6 b) describes the mean segmentation accuracy of DFC + SLDHOA-based DMN with a population size equal to 15. When using cluster sizes of 2, 3, or 5, the mean segmentation accuracy for the AD class type is 81.1 %, 80.8 %, 80.6 % and 80.3 %, respectively. Additionally, for MCI class type, the

mean segmentation accuracy assessed by DFC with cluster size = 2, 3, 4 and 5 are 88.4 %, 87.3 %, 85.3 % and 82.5 %, respectively. Fig. 6 c) depicts the sensitivity of DFC + SLDHOA-based DMN with a population size equal to 15. The sensitivity determined by DFC + SLDHOA-based DMN with hidden neurons = 100, 200, 300 and 400 is 52 %, 52.1 %, 54 % and 54.8 % for 50 % of the data, respectively. Additionally, for 90 % of data, the DFC + SLDHOA-based DMN with hidden neurons = 100, 200, 300 and 400 evaluated sensitivity is 77.9 %, 81.2 %, 82.5 % and 83.7 %, respectively. Fig. 6 d) depicts the specificity of DFC + SLDHOA-based DMN with a population size equal to 15. The specificity assessed by the DFC + SLDHOA-based DMN with the hidden neurons = 100, 200, 300 and 400 is 45.4 %, 47.9 %, 49.1 % and 49.7 % for 50 % of data, respectively. For 90 % of data, the specificity calculated by DFC + SLDHOA-based DMN by hidden neurons = 100, 200, 300 and 400 is 84.8 %, 86.7 %, 87.3 % and 88.7 %, respectively.

### 5.6. Comparative methods

The assessment was conducted using the following methodologies: DCF-RF [1], DFC + CNN [2], DFC-Sparse feature learning [3], DFC-Graph CNN [6], Underlying Knowledge-based Semi-Supervised Learning(UKSSL) [35], TL-CNN [7] and DFC + SLDHOA-based DMN.

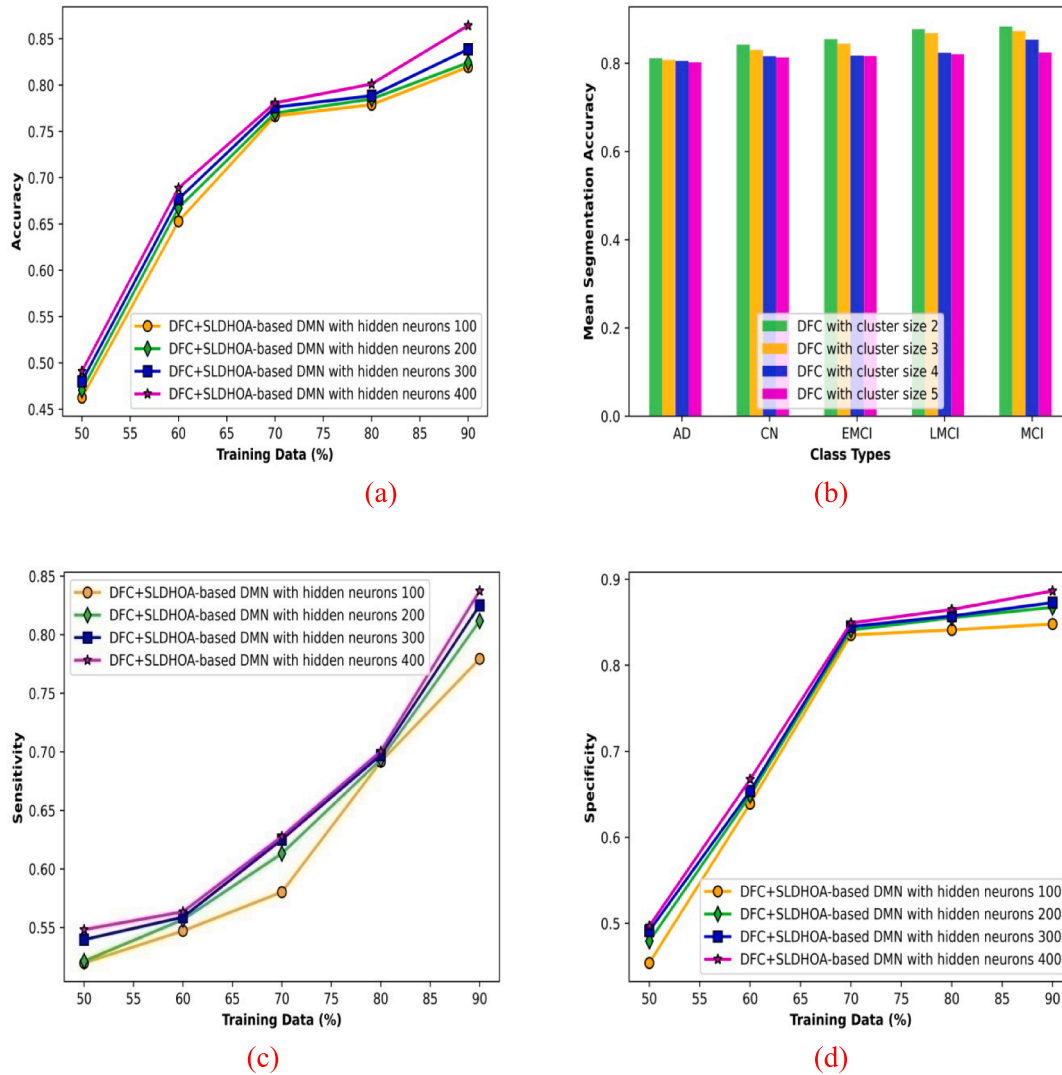


Fig. 6. Performance evaluation of DFC + SLDHOA-DMN with population size = 15 using a) Accuracy, b) mean segmentation accuracy, c) Sensitivity, and d) Specificity.

### 5.7. Comparative analysis

The evaluation of the existing approaches using sensitivity, specificity, and accuracy is illustrated by altering data using population sizes of 10 and 15.

#### 5.7.1. Assessment with population size = 10

The assessment of techniques with population size = 10 using accuracy, mean segmentation accuracy, sensitivity, and specificity is described in Fig. 7. The accuracy is displayed in Fig. 7a). In 50% of the training data, the accuracy evaluated by DCF-RF, DFC + CNN, DFC-Sparse feature learning, UKSSL, DFC-Graph CNN, TL-CNN and proposed DFC + SLDHOA-DMN are 0.500, 0.500, 0.500, 0.500, 0.500, 0.500 and 0.500. Also, in 90 % of training data, the accuracy evaluated by DCF-RF, DFC + CNN, DFC-Sparse feature learning, UKSSL, DFC-Graph CNN, TL-CNN and proposed DFC + SLDHOA-based DMN are 0.816, 0.844, 0.843, 0.849, 0.854, 0.861 and 0.874. The percentage improvement of DCF-RF, DFC + CNN, DFC-Sparse feature learning, UKSSL, DFC-Graph CNN, and TL-CNN concerning proposed DFC + SLDHOA-based DMN using accuracy are 6.636 %, 3.432 %, 3.546 %, 2.860 %, 2.288 % and 1.487 %. The mean segmentation accuracy is displayed in Fig. 7b.

For the AD class type, the mean segmentation accuracy evaluated by Global thresholding, FCM, DFCM, and proposed DFC are 0.811, 0.696, 0.791, and 0.881. Also, for MCI class type, the mean segmentation accuracy evaluated by Global thresholding, FCM, DFCM, and proposed DFC are 0.871, 0.733, 0.850, and 0.924. The percentage improvement of the proposed DFC using mean segmentation accuracy is 5.735 %, 20.670 %, 8 %. The sensitivity is displayed in Fig. 7c. For 50 % of data, the sensitivity of DCF-RF, DFC + CNN, DFC-Sparse feature learning, UKSSL, DFC-Graph CNN, TL-CNN and proposed DFC + SLDHOA-based DMN are 0.501, 0.534, 0.511, 0.528, 0.539, 0.557 and 0.593. Also, the training data are 90 %, the sensitivity evaluated by DCF-RF, DFC + CNN, DFC-Sparse feature learning, UKSSL, DFC-Graph CNN, TL-CNN and proposed DFC + SLDHOA-DMN are 0.733, 0.789, 0.775, 0.787, 0.809, 0.828 and 0.844. The improvement of DCF-RF, DFC + CNN, DFC-Sparse feature learning, UKSSL, DFC-Graph CNN, and TL-CNN concerning proposed DFC + SLDHOA-based DMN using sensitivity are 13.151 %, 6.516 %, 8.175 %, 6.754 %, 4.416 %, and 1.896 %. The specificity is displayed in Fig. 7d. For 50 % of data, the specificity of DCF-RF, DFC + CNN, DFC-Sparse feature learning, UKSSL, DFC-Graph CNN, TL-CNN and proposed DFC + SLDHOA-DMN are 0.500, 0.500, 0.500, 0.500, 0.500, 0.500 and 0.500. Also, for 90 % data, the specificity of DCF-RF, DFC +

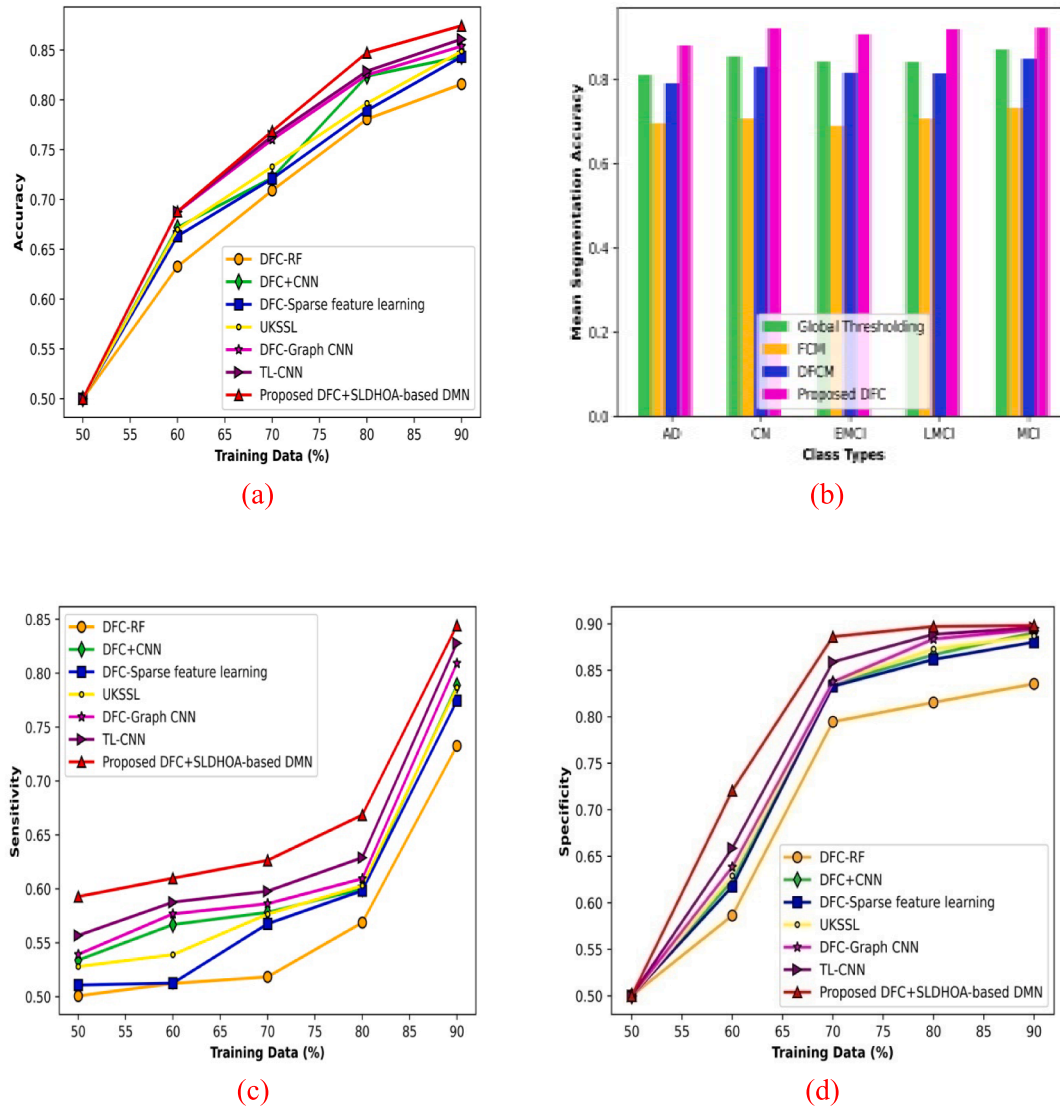


Fig. 7. Comparative assessment based on the techniques with population size = 10 using a) Accuracy b) mean segmentation accuracy c) Sensitivity d) Specificity.

CNN, DFC-Sparse feature learning, UKSSL, DFC-Graph CNN, TL-CNN and proposed DFC + SLDHOA-DMN are 0.835, 0.891, 0.880, 0.887, 0.894, 0.896 and 0.898. The improvement of performance in DCF-RF, DFC + CNN, DFC-Sparse feature learning, UKSSL, DFC-Graph CNN and TL-CNN for proposed DFC + SLDHOA-based DMN using specificity are 7.015 %, 0.779 %, 2.004 %, 1.225 %, 0.445 %, and 0.223 %.

5.7.2. Assessment with population size = 15

Fig. 8 presents the assessment of techniques with a population size of 15 using specificity, sensitivity, segmentation accuracy, and accuracy. The accuracy is displayed in Fig. 8a. For 50 % of data, the accuracy evaluated by DCF-RF, DFC + CNN, DFC-Sparse feature learning, UKSSL, DFC-Graph CNN, TL-CNN and proposed DFC + SLDHOA-DMN are 0.500, 0.500, 0.500, 0.500, 0.500, 0.500 and 0.500. Also, for 70% of the training data, the accuracy evaluated by DCF-RF, DFC + CNN, DFC-Sparse feature learning, UKSSL, DFC-Graph CNN, TL-CNN and proposed DFC + SLDHOA-based DMN are 0.759, 0.764, 0.760, 0.769, 0.772, 0.784, and 0.791. The significant improvement of DCF-RF, DFC + CNN, DFC-Sparse feature learning, UKSSL, DFC-Graph CNN, and TL-CNN concerning proposed DFC + SLDHOA-based DMN using accuracy are 4.046 %, 3.413 %, 3.919 %, 2.781 %, 2.402 %, and 0.885 %. The

mean segmentation accuracy is explained in Fig. 8b. For the AD class type, the mean segmentation accuracy evaluated by Global thresholding, FCM, DFCM, and proposed DFC are 0.832, 0.714, 0.813, and 0.879. Also, for MCI class type, the mean segmentation accuracy evaluated by Global thresholding, FCM, DFCM, and proposed DFC are 0.893, 0.749, 0.873, and 0.926. The improvement of the proposed DFC using mean segmentation accuracy is 3.563 %, 19.114 %, and 5.723 %. The sensitivity is displayed in Fig. 8c. For 50 % of training data, the sensitivity evaluated by DCF-RF, DFC + CNN, DFC-Sparse feature learning, UKSSL, DFC-Graph CNN, TL-CNN and proposed DFC + SLDHOA-DMN are 0.502, 0.534, 0.504, 0.519, 0.535, 0.547 and 0.579. Also, for 90% of the training data, the sensitivity of DCF-RF, DFC + CNN, DFC-Sparse feature learning, UKSSL, DFC-Graph CNN, TL-CNN and proposed DFC + SLDHOA-based DMN are 0.759, 0.808, 0.769, 0.788, 0.833, 0.836 and 0.839. The improvement of DCF-RF, DFC + CNN, DFC-Sparse feature learning, UKSSL, DFC-Graph CNN, and TL-CNN to proposed DFC + SLDHOA-DMN using sensitivity are 9.535 %, 3.694 %, 8.343 %, 6.079 %, 0.715 %, and 0.358 %. The specificity is displayed in Fig. 8d. For 50 % of data, the specificity of DCF-RF, DFC + CNN, DFC-Sparse feature learning, UKSSL, DFC-Graph CNN, TL-CNN and proposed DFC + SLDHOA-based DMN are 0.500, 0.500, 0.500, 0.500, 0.500, 0.500 and 0.500 and

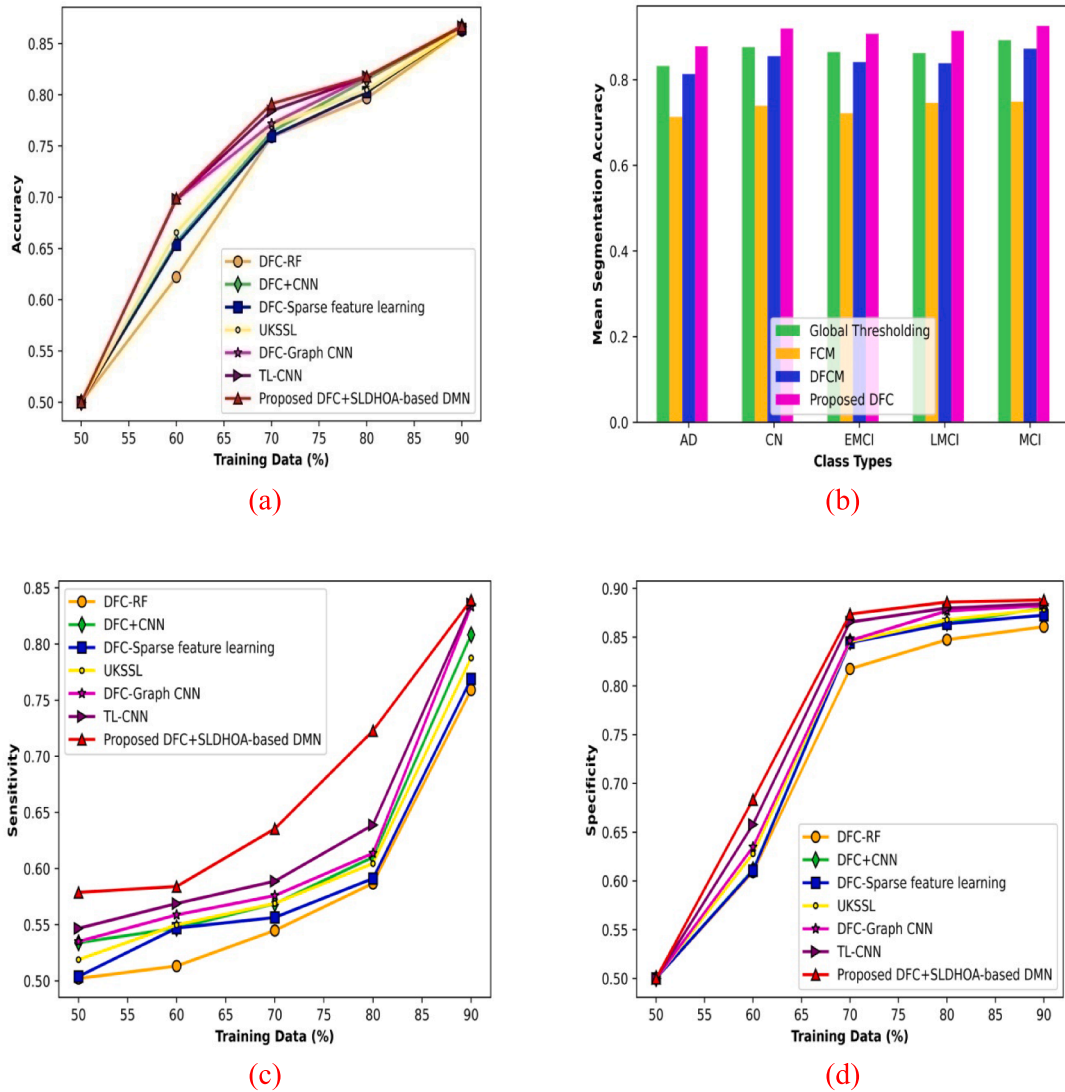


Fig. 8. Comparative assessment based on the techniques with population size = 15 using a) Accuracy b) mean segmentation accuracy c) Sensitivity d) Specificity.

Table 4  
Comparative analysis.

Population Size	Metrics	DFC-RF	DFC + CNN	DFC-Sparse feature learning	UKSSL	DFC-Graph CNN	TL-CNN	Proposed DFC + SLDHOA-based DMN
10	Accuracy (%)	81.6	84.4	84.3	84.9	85.4	86.1	87.4
	Sensitivity (%)	73.3	78.9	77.5	78.7	80.9	82.8	84.4
	Specificity (%)	83.5	89.1	88.0	88.7	89.4	89.6	89.8
15	Accuracy (%)	75.9	76.4	76.0	76.9	77.2	78.4	79.1
	Sensitivity (%)	75.9	80.8	76.9	78.8	83.3	83.6	83.9
	Specificity (%)	86.1	88.0	87.3	87.9	88.2	88.4	88.8

0.500. In 90% of the training data, the specificity evaluated by DCF-RF, DFC + CNN, DFC-Sparse feature learning, UKSSL, DFC-Graph CNN, TL-CNN and proposed DFC + SLDHOA-based DMN are 0.861, 0.880, 0.873, 0.879, 0.882, 0.884 and 0.888. The improvement of DCF-RF, DFC + CNN, DFC-Sparse feature learning, UKSSL, DFC-Graph CNN, and TL-CNN to proposed DFC + SLDHOA-based DMN using specificity are 3.040 %, 0.900 %, 1.689 %, 1.014 %, 0.675 %, and 0.45 %.

5.8. Discussion

Table 4 describes the comparative analysis using population sizes 10 and 15 by varying the training data. Here, the assessment is done using the population sizes 10 and 15. Using population size 10, the highest accuracy of 0.874 is measured by proposed DFC + SLDHOA-DMN while the accuracy evaluated by DCF-RF, DFC + CNN, DFC-Sparse feature

Table 5

Assessment based on segmentation accuracy.

Population size	Global thresholding	FCM	DFCM	Proposed DFC
10	0.871	0.733	0.850	0.924
15	0.893	0.749	0.873	0.926

learning, UKSSL, DFC-Graph CNN, and TL-CNN are 0.816, 0.844, 0.843, 0.849, 0.854, and 0.861. The highest sensitivity of 0.844 is evaluated by DFC + SLDHOA-DMN while the sensitivity evaluated by DCF-RF, DFC + CNN, DFC-Sparse feature learning, UKSSL, DFC-Graph CNN, and TL-CNN are 0.733, 0.789, 0.775, 0.787, 0.809, and 0.828. The highest specificity of 0.898 is measured by the proposed DFC + SLDHOA-based DMN while the specificity evaluated by DCF-RF, DFC + CNN, DFC-Sparse feature learning, UKSSL, DFC-Graph CNN, and TL-CNN are 0.835, 0.891, 0.880, 0.887, 0.894, and 0.896. Using population size 10, the highest accuracy of 87.4 %, the sensitivity of 84.4 % and specificity of 89.8 % are measured by the developed DFC + SLDHOA-DMN.

Table 5 describes the assessment of segmentation based on segmentation accuracy. Using population size 10, the highest segmentation accuracy of 0.924 is measured by the DFC and also, the segmentation accuracy is measured by global thresholding, FCM, and DFCM is 0.871, 0.733, and 0.850. Using population size 15, the highest segmentation accuracy of 0.926 is measured by the developed DFC while the segmentation accuracy measured by global thresholding, FCM, and DFCM is 0.893, 0.749, and 0.873.

## 6. Conclusion

For the classification of AD, the deep model is developed. The input images are first delivered into the pre-processing stage. To remove noise, the pre-processing is done with a Gaussian filter. After that, a modified DFC is used to segment the RoI, and the SLDHO is used to tune the DFC's hyperparameters. Here, DHOA and SlnO are combined to create the suggested SLDHO.CNN features, textual features like LGBP and SLIF, and statistical features such as variance, mean, skewness, kurtosis, energy, standard deviation, entropy and contrast are being mined. Based on DMN, the classification is carried out. Here, the created SLDHO is used for DMN training. The DMN further divides the AD into five categories: MCI, LMCI, EMCI, CN, and AD. With a maximum specificity of 89.8 %, sensitivity of 84.4 % and accuracy of 87.4 % increase the performance of the DFC-SLDHO-DMN. Further, the segmentation accuracy is evaluated based on the segmentation techniques, in which the value of the highest segmentation accuracy is 0.926. The major limitations of the proposed method are, that a limited dataset is used to find the AD, which provides high accuracy but the result is in poor generalization. Also, this work only considered the MRI scan images to detect AD. Moreover, the Gaussian filter has the limitation of reducing details, this will be done in further study. Also, the future work will aim to identify other types of images like Computed Tomography (CT), ultrasound images, and X-ray images. Moreover, another dataset will be adapted for feasibility check of the proposed model and the real-time implementation will also considered in future.

## CRedit authorship contribution statement

**T.S. Sindhu:** Conceptualization, Writing – original draft, Writing – review & editing, Visualization, Investigation. **N. Kumaratharan:** Supervision, Project administration.

## Declaration of competing interest

The authors declare that they have no known competing financial interests or personal relationships that could have appeared to influence the work reported in this paper.

## Data availability

<https://www.kaggle.com/madhucharan/alzheimersdisease5classdatasetadni>

## References

- [1] M. Song, H. Jung, S. Lee, D. Kim, M. Ahn, Diagnostic Classification and Biomarker Identification of Alzheimer's Disease with Random Forest Algorithm, *Brain Sci.* 11 (4) (2021) 453.
- [2] J.B. Bae, S. Lee, W. Jung, S. Park, W. Kim, H. Oh, J.W. Han, G.E. Kim, J.S. Kim, J. H. Kim, K.W. Kim, Identification of Alzheimer's disease using a convolutional neural network model based on T1-weighted magnetic resonance imaging, *Sci. Rep.* 10 (1) (2020) 1–10.
- [3] L. Xu, Z. Yao, J. Li, C. Lv, H. Zhang, B. Hu, Sparse feature learning with label information for Alzheimer's disease classification based on magnetic resonance imaging, *IEEE Access* 7 (2019) 26157–26167.
- [4] Y. Zhang, S. Wang, K. Xia, Y. Jiang, P. Qian, and Alzheimer's Disease Neuroimaging Initiative, Alzheimer's disease multiclass diagnosis via multimodal neuroimaging embedding feature selection and fusion, *Inform. Fusion* 66 (2021) 170–183.
- [5] X. Bi, X. Zhao, H. Huang, D. Chen, Y. Ma, Functional brain network classification for Alzheimer's disease detection with deep features and extreme learning machine, *Cogn. Comput.* 12 (3) (2020) 513–527.
- [6] H. Padole, S.D. Joshi, T.K. Gandhi, Graph wavelet-based multilevel graph coarsening and its application in graph-CNN for Alzheimer's disease detection, *IEEE Access* 8 (2020) 60906–60917.
- [7] S. Afzal, M. Maqsood, F. Nazir, U. Khan, F. Aadir, K.M. Awan, I. Mehmood, O. Y. Song, A data augmentation-based framework to handle class imbalance problem for Alzheimer's stage detection, *IEEE Access* 7 (2019) 115528–115539.
- [8] T. Zhu, C. Cao, Z. Wang, G. Xu, J. Qiao, Anatomical Landmarks and DAG Network Learning for Alzheimer's Disease Diagnosis, *IEEE Access* 8 (2020) 206063–206073.
- [9] J.C. Millán-Calenti, L. Lorenzo-López, B. Alonso-Búa, C. De Labra, I. González-Abrales, and A. Maseda, Optimal nonpharmacological management of agitation in Alzheimer's disease: challenges and solutions Clinical interventions in Aging, 11 (2016) 175.
- [10] D.K. Lahiri, M.R. Farlow, N.H. Greig, K. Sambamurti, Current drug targets for Alzheimer's disease treatment, *Drug Dev. Res.* 56 (3) (2002) 267–281.
- [11] F.J. Martínez-Murcia, J.M. Górriz, J. Ramírez, F. Segovia, D. Salas-Gonzalez, D. Castillo-Barnes, I.A. Illán, A. Ortiz, and Alzheimer's Disease Neuroimaging Initiative, Evaluating Alzheimer's disease diagnosis using texture analysis, in: *In Annual Conference on Medical Image Understanding and Analysis*, 2017, pp. 470–481.
- [12] R. Brookmeyer, E. Johnson, K. Ziegler-Graham, H.M. Arrighi, Forecasting the global burden of Alzheimer's disease, *Alzheimers Dement.* 3 (3) (2007) 186–191.
- [13] M. Grundman, R.C. Petersen, S.H. Ferris, R.G. Thomas, P.S. Aisen, D.A. Bennett, N. L. Foster, C.R. Jack Jr, D.R. Galasko, R. Doody, J. Kaye, Mild cognitive impairment can be distinguished from Alzheimer disease and normal ageing for clinical trial, *Arch. Neurol.* 61 (1) (2004) 59–66.
- [14] A. Esteva, B. Kuprel, R.A. Novoa, J. Ko, S.M. Swetter, H.M. Blau, S. Thrun, Dermatologist-level classification of skin cancer with deep neural networks, *Nature* 542 (7639) (2017) 115–118.
- [15] L. Fang, Z. Yao, J. An, X. Chen, Y. Xie, H. Zhao, J. Mao, W. Liang, X. Ma, Topological organization of metabolic brain networks in pre-chemotherapy cancer with depression: a resting-state PET study, *PLoS One* 11 (11) (2016) e0166049.
- [16] Y. Zhang, S. Wang, P. Phillips, Z. Dong, G. Ji, J. Yang, Detection of Alzheimer's disease and mild cognitive impairment based on structural volumetric MR images using 3D-DWT and WTA-KSVM trained by PSOTVAC, *Biomed. Signal Process. Control* 21 (2015) 58–73.
- [17] G.B. Frisoni, N.C. Fox, C.R. Jack, P. Scheltens, P.M. Thompson, The clinical use of structural MRI in Alzheimer disease, *Nat. Rev. Neurol.* 6 (2) (2010) 67–77.
- [18] J. Peng, L. An, X. Zhu, Y. Jin, and D. Shen, Structured sparse kernel learning for imaging genetics based Alzheimer's disease diagnosis, in: *Proceedings of International Conference on Medical Image Computing and Computer-Assisted Intervention*, (2016) 70–78.
- [19] F.J. Martínez-Murcia, A. Ortiz, J.M. Górriz, J. Ramirez, D. Castillo-Barnes, Studying the manifold structure of Alzheimer's disease: A deep learning approach using convolutional autoencoders, *IEEE J. Biomed. Health Inform.* 24 (1) (2019) 17–26.
- [20] M. Liu, J. Zhang, E. Adeli, D. Shen, Landmark-based deep multi-instance learning for brain disease diagnosis, *Med. Image Anal.* 43 (2018) 157–168.
- [21] M. Liu, D. Zhang, D. Shen, and Alzheimer's Disease Neuroimaging Initiative, "Ensemble sparse classification of Alzheimer's disease, *Neuroimage* 60 (2) (2012) 1106–1116.
- [22] R. Cui, M. Liu, G. Li, Longitudinal analysis for Alzheimer's disease diagnosis using RNN, in: *Proceedings of 2018 IEEE 15th International Symposium on Biomedical Imaging (ISBI 2018)*, 2018, pp. 1398–1401.
- [23] I. Beheshti, N. Maikusa, H. Matsuda, H. Demirel, G. Anbarjafari, Histogram-based feature extraction from individual grey matter similarity-matrix for Alzheimer's disease classification, *J. Alzheimers Dis.* 55 (4) (2017) 1571–1582.
- [24] W. Sun, F. Su, L. Wang, Improving deep neural networks with multi-layer maxout networks and a novel initialization method, *Neurocomputing* 278 (2018) 34–40.
- [25] Q. Feng, L. Chen, C.P. Chen, L. Guo, Deep Fuzzy Clustering—A Representation Learning Approach, *IEEE Trans. Fuzzy Syst.* 28 (7) (2020) 1420–1433.

- [26] G. Brammya, S. Praveena, N.S. NinuPreetha, R. Ramya, B.R. Rajakumar, D. Binu, Deer hunting optimization algorithm: a new nature-inspired meta-heuristic paradigm, *Comput. J.* (2019).
- [27] R. Masadeh, B.A. Mahafzah, A. Shariah, Sea lion optimization algorithm, *Sea* 10 (5) (2019).
- [28] W. Zhang, S. Shan, W. Gao, X. Chen, and H. Zhang, Local gabor binary pattern histogram sequence (LGBPHS): A novel non-statistical model for face representation and recognition, in: *Proceedings of Tenth IEEE International Conference on Computer Vision (ICCV'05)*, 1 (2005) 786-791.
- [29] F. Fausto, E. Cuevas, A. Gonzales, A new descriptor for image matching based on bionic principles, *Pattern Anal. Appl.* 20 (4) (2017) 1245-1259.
- [30] Alzheimers-Disease-5-Class-Dataset-ADNI taken from, <https://www.kaggle.com/madhucharan/alzheimersdisease5classdatasetadni>. accessed .on July 2021.
- [31] J.J. Hwang, and K.H. Rhee, Gaussian filtering detection based on features of residuals in image forensics, in: *IEEE RIVF International Conference on Computing & Communication Technologies, Research, Innovation, and Vision for the Future (RIVF)*, (2016) 153-157.
- [32] D. Mungra, A. Agrawal, P. Sharma, S. Tanwar, M.S. Obaidat, PRATT: a CNN-based emotion recognition system using histogram equalization and data augmentation, *Multimed. Tools Appl.* 79 (3) (2020) 2285-2307.
- [33] Data augmentation, <https://machinelearningmastery.com/image-augmentati-on-deep-learning-keras/>. Accessed on September 2021.
- [34] A. Sarkar, Optimization Assisted Convolutional Neural Network for Facial Emotion Recognition, *Multimedia Research* 3 (2) (2020).
- [35] Z. Ren, X. Kong, Y. Zhang, S. Wang, UKSSL: Underlying Knowledge based Semi-Supervised Learning for Medical Image Classification, *IEEE Open J. Eng. Med. Biol.* (2023).
- [36] Z. Ren, S. Wang, Y. Zhang, Weakly supervised machine learning, *CAAI Trans. Intelli. Technol.* (2023).
- [37] Y. Zhang, L. Deng, H. Zhu, W. Wang, Z. Ren, Q. Zhou, S. Lu, S. Sun, Z. Zhu, J. ManuelGorri, S. Wang, Deep learning in food category recognition, *Information Fusion* 98 (2023).